# Catalysis Science & Technology

Accepted Manuscript






ROYAL SOCIETY OF CHEMISTRY

www.rsc.org/catalysis

Catalysis
Science & Technology

RSCPublishing

ARTICLE

# Washcoating of Cordierite Honeycomb with Vanadia-Tungsta-Titania Mixed Oxides for Selective Catalytic Reduction of NO with $NH_3$

Bo Liu, Jun Du*, Xiaowei Lv, Yue Qiu, Changyuan Tao

The application of monolithic coated catalysts to the $NO_x$ abatement is a crucial issue for practical applications to enhance mechanical strength, economize cost, facilitate to recycling etc, compared with the conventional monolithic extrusive ones. In the present work, cordierite honeycomb monoliths coated with V, W and Ti elements catalyst were synthesized, characterized and tested in the selective catalytic reduction (SCR) NO with $NH_3$. The coating process conduced a highly dispersing of active species, generated an enrichment of tungsta and vanadia on surface of the coating. Raman and UV-vis DRS spectrum confirmed the speciations of vanadia, which were mainly presented in isolated state with a large proportion of 88.68%, the others were found in polymeric state possessing one mono-oxo V=O terminal band and three bridging V-O-M bands (M=V or support cation). XPS indicated co-exist of pentavalent vanadium and tiny proportion of tetravalent vanadium. The layer coated onto the cordierite substrate possessed a homogeneous distribution with a strong adherence and a deep penetration with catalytic components dipping into cordierite. The coated monolithic catalyst exhibited a desired catalytic performance exceeding 90% of NO removal rate in the range of 350 to 450 ℃ and a strong tolerance of poisoning in sulfur and moisture in $NH_3$-SCR reaction.

## Introduction

A well-establish technology for eliminating harmful NO from stationary emission sources is the selective catalytic reduction (SCR) with $NH_3$. The catalyst employed for common commercialized industrial consisted primarily of monolithic extruded $V_2O_5$+$WO_3$($MoO_3$)/$TiO_2$ catalyst, which was operated under 300–450 ℃, and substantial work had been done to improve the performance of vanadium type catalysts.[1] While, anecdotal evidence had suggested that monolithic supported catalysts presented many advantages like greater mechanical strength, more excellent heat transfer performance, higher catalytic performance with less active components and faster response to changing conditions etc.[2-4]

The most common and popular material for monolithic structures is cordierite honeycomb ceramics which consists of magnesia, silica, and alumina in ratio of 2:5:2 and single blocks of small parallel, non-intersecting channels.[4] In reference to ceramic monoliths, the support presents excellent operational properties, such as high mechanical strength, high temperature resistance, low thermal expansion coefficient, low pressure drop and available in various sizes or shapes.[5] Usually different procedures could be performed in coating the monolith walls with support materials called washcoat like γ-$Al_2O_3$, $TiO_2$, $ZrO_2$ or zeolites to obtain a higher surface area and abundant pore since cordierite itself exhibits negligible porosity and nearly has no contribution to catalytic action.[6] Regarding the deposition method for active phases, different strategies, like hydrothermal synthesis, sol-gel process, chemical vapor deposition and dip-coating have been employed for initially coating the monolith channels with an additional support material, then followed by the accretion of active phases to the coating of a ready-made catalyst.[7] The combination forces between the coating layer and the substrate are usually one of the key issues for developing high performance catalysts. Further more, the tuning or controlling of the active species distribution and anchoring mechanism onto the substrate could act as an effective way for approaching the prospective catalytic effect. This coated monolithic catalyst would provide us an alternative way for industrial catalyst molding and easy to obtain divers heterogeneous catalysts, also an prospective way for catalyst recycling instead of solid waste disposal.

In the present study, we developed an coated monolithic cordierite catalyst with the application of the titania sols and

molded honeycomb cordierite, followed by the impregnation of vanadia and tungsten. We investigated the textural and morphologies of the coated catalyst, as well as the combination of coating and substrate, distribution of the active species and redox properties of washcoat based on the utilizing of various characterization methods. The catalytic performance of the catalyst in $NH_3$-SCR reaction for the removing of nitrogen monoxide had been evaluated and correlated with the catalyst structure.

## Experimental

### Preparation of monolithic coated catalysts

**Pretreatment of cordierite.** A commercial cordierite honeycomb monoliths with type of cell density 3 cpsi and square channels (150 mm × 150 mm of section and 350 mm long) are used as substrate. Before coating, all the resulted samples are swilled by tap water to remove soluble impurities and the dust produced in the cutting process. Then wash the resulted monoliths thoroughly with distilled water, further to be dried in oven 80 ℃ for 6 hours and coasted in static air in muffle furnace 300 ℃ for 3 hours with the aim of removing organic impurities.

**Preparation of sols.** The titania sol are prepared using precursor of tetrabutyl titanate in a certain process where dissolved tetrabutyl titanate in ethanol and added dropwise deionized water together with inhibitors and catalyzers under constant stirring (300 r/min) into three-necked flask at room temperature for 2 hours. The titania sol possesses a properties of 8.13 nm of average grain diameter, 10.3 mpa.s of viscosity, 0.9622 g/mL of density, -1.11 mV of zeta potential, 10.35 wt% of $TiO_2$ content and pH=4. The mixed metal oxides sols are made in a similar way of titania sol except dissolving additional precursors of metal oxides into deionized water, then adding dropwise into corresponding sols. The W-Ti sol consists 4.8 wt% tungsten, V-W-Ti sol consists 0.8 wt% vanadium and 4.8 wt% tungsten and V-Ti sol consist 0.8 wt% vanadium.

**Preparation of impregnation solutions.** Dissolve precursor of metal oxides into deionized water to obtain the impregnation liquids. The vanadia solution possesses a concentration of 0.8 wt%, tungsten solution is 4.8 wt% and V-W solution is 0.8 wt% vanadium and 4.8 wt% tungsten.

**Preparation of coated catalysts.** Put the resulted cordierite monolith immerse into titania sol and V-W impregnation solution suspensions to deposit support material and active components. Whereafter, unclogging of the channels should be performed using an aurilave, prior to the resulting washed samples are submitted into oven 80 ℃ for 2 hours to evaporate the water and the volatile organic solvents existed in the washcoated monoliths. The resulted monolith are transferred to a muffle furnace calcination 450 ℃ for 3h and further to be labeled V-W/Ti/CC, where CC referred to cordierite.

In accordance with the method of V-W/Ti/CC to synthesis V/W-Ti/CC, W/V-Ti/CC, V/Ti/CC, Ti/CC, where W-Ti, V-Ti and Ti referred to W-Ti sol, V-Ti sol and $TiO_2$ sol, respectively. Besides, the sample of $TiO_2$ and V-W-Ti are prepared by calcinating corresponding sols.

### Catalyst performances

All of the cordierite monolith catalyst samples are crushed and sieved to 16-40 mesh for test in the $NH_3$-SCR reaction in a self-made continuous flow stainless tube reactor coupled to a chemiluminescence NO analyzer which is used to detect the concentration of NO from effluent gas under atmospherically relevant conditions. Prior to testing, the catalyst is first actived at 250□ oxygen (5%) atmosphere. The feed stream consists, in all cases, of 500 ppm NO, 500 ppm $NH_3$, 2 vol% $O_2$, $N_2$ as the balance, and a gas hourly space velocity (GHSV) of 6000 $h^{-1}$. Reactor temperature is increased from 250□ to 450□. NO conversion ($\eta_{NO}$) is calculated by measuring the concentration of the NO before ($C_{NO}^{in}$) and after ($C_{NO}^{out}$) the catalyst according to the following equation:

$$\eta_{NO} = \frac{C_{NO}^{in} - C_{NO}^{out}}{C_{NO}^{in}} \times 100\%$$

### Characterization techniques

The adherence of the washcoated phase is represented in terms of weight loss ($\Delta w$) after exposure of the monoliths to ultrasonic treatment (China, Model DY-4.5-180DT). The $\Delta w$ is calculated by measuring the weight of the catalyst before ($w_b$) and after ($w_a$) the ultrasonic treatment according to the following equation:

$$\Delta w = \frac{w_b - w_a}{w_b} \times 100\%$$

The morphology of cordierite monoliths catalyst are characterized by FE-SEM (JSM-7800F, JEOL, Japan).

The surface areas are measured by $N_2$ adsorption method on Micromeritics ASAP 2010M V3.00H instrument. Prior to nitrogen physisorption the samples are vacuumized at 300 ℃ for 4h to remove adsorbed impurities. Surface area is calculated using the BET equation ($S_{BET}$) in 0.05~0.2 relative pressure range. Pore volumes, average pore diameters, and pore size distributions are determined by Barrett-Joyner-Halenda (BJH) method form the $N_2$ desorption data.

The X-ray diffraction (XRD) patterns of the monoliths are measured on a Rigaku D/max-3C diffractometer, using the Cu K$\alpha$ radiation resource ($\lambda$ =1.54 Å) with a step size of 0.02°/s, scanning rate of 10°/min, 2$\theta$ varying from 5° to 90°, 40kV tube voltage and 30 mA tube current. The average crystal domain size of crystallite size (D) is estimated with the Scherrer equation:

$$D = \frac{0.89\lambda}{\beta \cos\theta}$$

Where $\theta$ is the diffraction angle of peak, and $\beta$ is the full width at half-maximum (FWHM) of the peak in radian, which is calibrated from high purity silicon.

Element analyses of the samples are analyzed by means of X-ray fluorescence (XRF, LAB CENTER XRF-1800, Shimadzu).

The X-ray photoelectron spectroscopy (XPS) analysis is performed using a Kratos AXIS Ultra DLD (Thermo ESCAlab 250) under ultra high vacuum using monochromated Al Kα source (1486.6 eV) at 450 W (30 mA, 15kV). Measurements are performed using 20 eV pass energy, 0.1 eV step and 0.15 dwelling time. Energy correction is carried out using the C1s signal of adventitious surface carbon C referenced at 285 eV.

Raman spectra are collected on a Horiba in LabRAM HR Evolution with a 532 nm laser as the excitation source, and in a range 100-1200 $cm^{-1}$ at room temperature. A laser output of 30 mW is employed and the maximum incident power at the sample is approximately 6 mW.

The UV-vis diffuse reflectance spectra of the catalysts are recorded in the range 200–800 nm at room temperature (SBW: 1 nm) using a UV-Vis spectrophotometer (TU-1901) equipped with an integration sphere (IS19-1). Reflectance data are converted to absorption spectra using Kubelka–Munk function. Prior to recording DRUV-Vis spectra the samples are dehydrated in oven at 80 ℃ for 12 h.

## Result and Discussion

### Test of Coating Stability

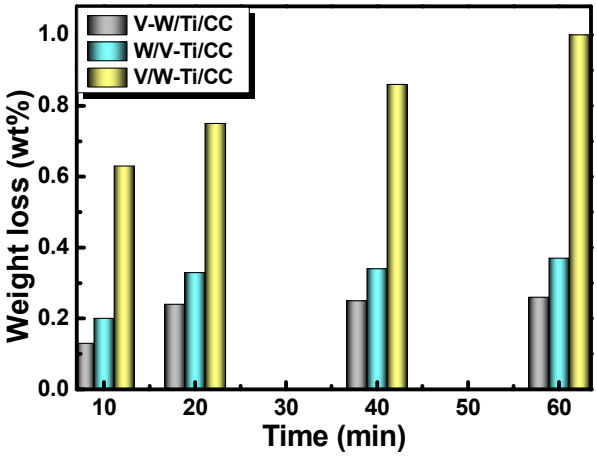


Fig. 1 V-W/Ti/CC catalyst weight loss over time under standard ultrasonic testing conditions.

The as-prepared catalysts showed considerable adhesive strength of the washcoat. The weight loss of the washcoat was less than 1 wt% for all samples (Fig. 1), indicating a strong adhesion between coating and cordierite substrate. Meanwhile, adhesive strength of the washcoat are obviously influenced by the catalyst preparation. Sample V/W-Ti/CC exerted a dramatic coating shedding. The W/V-Ti/CC and V-W/Ti/CC showed a similar ratio of slight coating weight loss. It can be speculated that coated tungsta generated a bonding reliability with titania support and cordierite substrate, which was stronger than that of vanadia. As far as we know, it facilitated multiple oxide species to form a more homogeneous distribution and a highly dispersion among different materials utilizing co-impregnation method, while aggregation in process of step impregnation. Hence, the binary oxides sol dipping could be easier to form an interaction force among internal evenly distributed materials, which was obviously superior to one-component in enhancing adhesion force between washcoat and substrate. Therefore the overall amount of coating weight loss, in large scale, depended on the adhesive ability of single active material with supports. We confirmed that tungsta owning a stronger combining capacity with supports than vanadia since W/V-Ti/CC present a fewer weight loss than that of V/W-Ti/CC. Furthermore, tungsten exhibited a synergistic effect with vanadium in co-impregnation since V-W/Ti/CC demonstrated an approximate washcoat weight loss relative to W/V-Ti/CC. In short all the coated sample possessed a desired washcoat adhesion.

### Catalyst Morphologies and Structural Characterizations

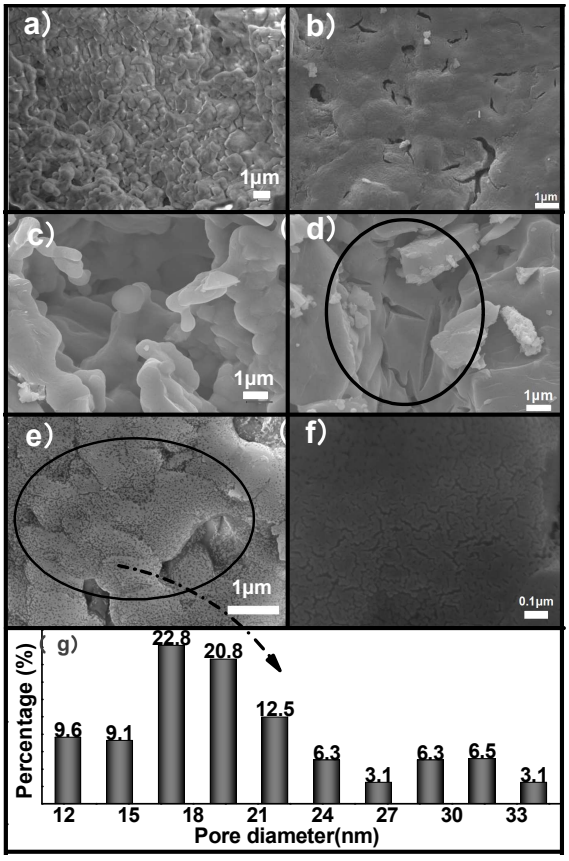


Fig. 2 SEM image of cordierite surface (a), cross sectional (c) and coated cordierite surface (b), cross sectional (d) and acid etched cordierite surface (e), cross sectional(f), pore size distributions (g).

**SEM.** Fig. 2 depicted the surface morphologies of V-W/Ti/CC catalyst investigated by SEM. As it can be seen from images above, the bare cordierite presented a compact grain arrange surface (Fig. 2a) and circular macropores (Fig. 2c). The resulted washcoat with a coating layer thickness of ca. 30 $\mu$m did not arise obvious cracking and peeling on the substrate surface for the impact of contraction stress caused by the temperature variations between the coating and the substrate surface, instead of a homogeneous distribution of the coating phase (Fig. 2b). Only a tiny proportion of cordierite elements (ca. Mg+Al+Si 2.5 at%) were detected according to EDS line scanning results of catalyst surface, which indicated almost all the cordierite was coated by layer (Supporting information). Due to the thermal fluctuation during catalyst diffusion annealing,[8] thin film layer surface atoms in a state of relative relaxation for the absence of adjacent atoms, and they obtain enough heat energy to disturb previous equilibrium state to diffuse, reunite, crystallize, and then generate grain boundaries coupling with thin film layer turning flat to bend, saw from Fig. 2b.

SEM image of cross sectional (Fig. 2d) depicted a washcoat with cracks cohered in the internal pore of cordierite, indicating that the catalyst components had infiltrated into cordierite substrate, which would generate a strong cohesive force between coating and substrate. As we know, the sol particles possessed an average pore size of 8 nm and existed in a organic system which have low surface tension and appropriate fluidness, therefore sols particles could be easily inlaid into the

honeycomb ceramic pore structure to achieve an effective combination and ensure an intensity of the new combination. And it has already been proved by EDS that vanadium, titanium and tungsten were found from cross section of the catalyst by detecting a line there (Supporting information).

Generally, except for removing soluble impurities and the dust produced in the cutting process by water scrubbing, CC usually underwent a step of acid corrosion for the aims of enhancing its porosity and specific surface area. Shigapov[9] et al found that further abundant pores and high surface area cordierite could be obtained through acid etch by dissolving some of MgO and $Al_2O_3$. Liu Q[10] et al showed that acid wash not simply increase the surface areas and pore volumes of cordierites, but promote the dispersion of active components and the activities of catalysts. Nevertheless, it should be pointed out that, for the catalyst treated in oxalic acid for over 12 h, its mechanical strength was visually low, which presented an extremely adverse effect toward the practical application of monolith catalysts. The procedure of acid treatment was not adopted in our study, however, both nano titanium sol and vanadium-tungsten aqueous solution exhibited acidic character which could corrode CC during the process, where the CC was continuously impregnated and dehydrated for a long time. To clear the influence of acidic impregnation situation, the impregnation liquids and sol were substituted by an oxalate solution possessing a same acidic property with them to simulate the process of preparing V-W/Ti/CC catalyst, which could provide a direct description about the influence.

As illustrated in the picture of acid corrosive cordierite surface (Fig. 2e) and cross sectional (Fig. 2f), plenty of wormlike mesopores and micropores did arises after the particular impregnation process, which demonstrated the acidic impregnation liquids facilitated to coating through creating more highly variable pores. The size correlates well with the wormlike pores was measured definitely by the Nano measure 1.2.0 software and displayed with a bar diagram (Fig. 2g) which clearly gave a proportion of different pores. However, the macopores were unable to present in the enlarge image from the acid treated cordierite towards its surface, the meso apertures in the image were ranging from 11 to 35 nm and the most diameter was about 17 nm.

Table 1 Structural parameters of different samples.

| Samples | $S_{BET}$ ($m^2 \cdot g^{-1}$)[a] | Pore volume ($cm3 \cdot g^{-1}$)[b] | Pore diameter (nm)[c] |
|---|---|---|---|
| **cordierite** | 0.0055 | ---- | ---- |
| **$TiO_2$** | 42.31 | 0.0490 | 4.44 |
| **Ti/CC** | 4.08 | 0.00569 | 5.33 |
| **V-W-Ti** | 72.45 | 0.0686 | 3.45 |
| **V-W/Ti/CC** | 7.21 | 0.00662 | 3.96 |

[a] BET Specific surface area
[b] BJH desorption pore volume
[c] Average pore diameter

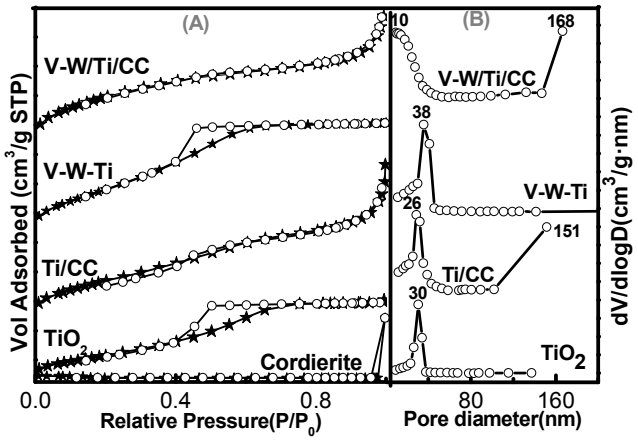


Fig. 3 $N_2$ adsorption-desorption isotherms and and pore size distributions of different samples.

**BET.** We further investigated the morphology of catalysts internal structures and influence of the coating process on pores distribution over coated catalysts. The $N_2$ adsorption-desorption isotherms were displayed in graphical form combining with the pore size distribution plotted against the differential pore volume ($cm^3/g \cdot nm$), where differential was the first order differential of the desorption isotherms. And the structural parameters of different samples were summarized in Table 1.

From the nitrogen isotherms (Fig. 3A), we learned that CC revealed negligible porosity and pore specific surface area, which could hardly be measured by $N_2$ adsorption[11] and were consistent with the results of SEM. Therefore, it could be reasonable to assume that there was no contribution of the CC support to the adsorption properties of the coated catalysts. Pure titania (sample $TiO_2$) illustrated a type IV nitrogen isotherm with a limiting uptake over a range of high $P/P_0$ and Type $H_2$ loop with a narrow distribution of pore size, according to the IUPAC classification.[12] The pronounced hysteresis taking place in mesopore structures in the multilayer range of physisorption isotherms was usually associated with capillary condensation which could cause desorption of the materials filling in pores when lagging behind the filling pressure, and signify that the pores were in 3D intersection networks.[13] The V-W-Ti sample offered a similar nitrogen isotherm as the sample of $TiO_2$, but revealed a rapid leap in BET specific surface area compared with that of $TiO_2$, from 42.31 to 72.45 $m^2 \cdot g^{-1}$, and a broader pore size distribution, indicating that the addition of vanadia and tungsta species increased the specific surface area of the catalyst dramatically.

Additionally, process of coating clearly offered influences respecting the properties of previous samples.

First, in comparison to the $TiO_2$ and V-W-Ti, there were a striking slump in specific surface area, micropore surface area and total volume of samples, and a broader and more in-depth pore size distribution with sundry ratios of micropores, mesopores and macropores over their coated samples. Particularly, the sample of V-W/Ti/CC possessed a crystal-clear broad distribution of pore in size than that of Ti/CC, which probably was due to the reasons that the species of vanadium and tungsten deposited into the titanium layer fall off and clog the pore canals, giving rise to the generation of pores with smaller size, and that the collapse of holes created apertures with larger size since the stress of membrane crack when heated. Furthermore, CC substrate supported no contribution to

the adsorption properties of the catalyst, consequently, the specific surface area of coated samples decreased when the titania washcoat was done over monolith. To put it like this, only 8.9 percentage of the layer was took up the whole catalyst, which lead to the specific surface area of sample V-W/Ti/CC sank to 4.08 from 42.31 $m^2 \cdot g^{-1}$.

Second, the plot of cumulative surface area against pore diameter (supporting information) over coated samples showed more than 90% of the total inner surface area available were mainly of micropores and mesopores less than 40 nm in diameter.

Last, in terms of judging the pore morphology, it was unwise to attribute their isotherms into type II which was a typical physical adsorption process over adsorbents with macropore or nonporous surfaces, rather than type IV in same certain respects, even though the isotherm did not rise faster under the medium relative pressure where the hysteresis loop should appear appreciably, and arise unrestricted monolayer-multilayer adsorption over a range of high $P/P_0$. Since there was no inevitable relationships between the formation of hysteresis loop and the existence of mesopores. Generally, the mesopores sharp correlated well with the hysteresis loop shape, the more inhomogenous of the pore cross section diameter, the more obvious of the hysteresis loop, which could be illustrated by the fact that the 'ink bottle' pores indicated a distinct hysteresis loop while the cylinder bores exerted barely hysteresis loop. In this study polts of corresponding pore size distribution over the coated samples displayed a mainly apertures in mesoporous size. Consequently, the physisorption isotherms of the coated samples were classed as the type IV.

Briefly, we concluded that the dip-coating procedure used to prepare coated catalysts was unable to modify the previous porosity of washcoat significantly. Besides micropores and mesopores in the coated samples would play an important role in supplying sites for both adsorption and SCR surface reactions,[14] and the mass transfer was much easier with the existence of some macropores.[15]

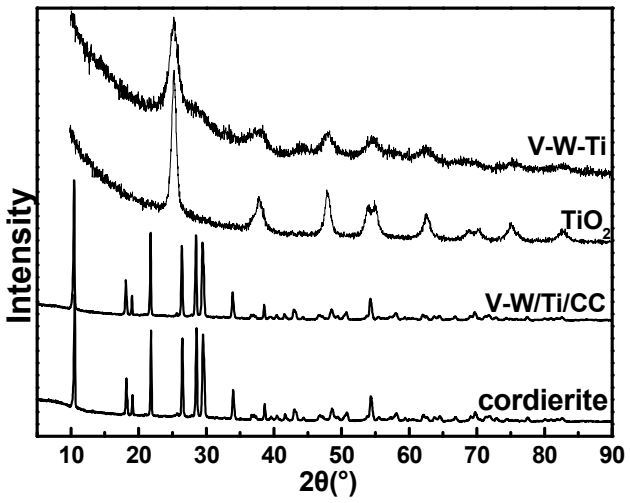


Fig. 4 XRD results of different samples.

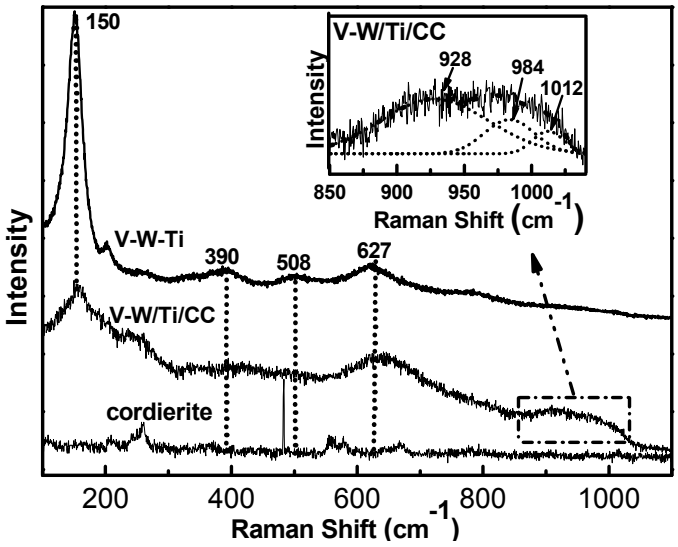


Fig. 5 Raman results of different samples.

**XRD and Raman.** The XRD results of the obtained samples are displayed in Fig. 4, and the magnification factor of all the XRD patterns given in the graph is twice. It can be seen from the XRD patterns of $TiO_2$ sample that the reflection peaks characteristic of anatase phases (PDF2004: 00-021-1272) were exhibited, as expected. While, only the broad diffraction peaks attributed to anatase $TiO_2$ can be observed in the XRD pattern of V-W-Ti. The characteristic lines corresponding to vanadia and tungsta were absent, which suggested that $V^{5+}$ and/or $W^{6+}$ had been successfully incorporated into the lattice of anatase $TiO_2$ to form uniform solid solution maintaining the anatase crystal form.[16] The average crystallite size (D) of $TiO_2$ sample, calculated by the Sherrer formula, was reduced from 13.31 to 7.17 nm compared with sample V-W-Ti. And we can notice that the diffraction peaks of V-W-Ti were broader than those of anatase $TiO_2$ owing to the decrease of crystallite size, which indicated that the introduction of $V^{5+}$ and/or $W^{6+}$ into the lattice of anatase $TiO_2$ may inhibited its grain growth. Interestingly, it can be noted from Table 1 that the BET specific surface area of V-W-Ti (72.45 $m^2 \cdot g^{-1}$) was obviously larger than that of anatase $TiO_2$ (42.31 $m^2 \cdot g^{-1}$), indicating that the incorporation of $V^{5+}$ and/or $W^{6+}$ into the lattice of anatase $TiO_2$ can improve its texture property effectively. This was consistent with the results of SEM.

Furthermore, exposure of the V-W/Ti/CC catalyst to XRD spectra for crystal morphology information of phase layer cannot result in any valuable conclusions except suggesting an intense crystal peak of cordierite (PDF2004: 01-089-1487) alone, and the same to all other coated catalysts (not given). This could be attributed to the reasons that the strong CC peaks covered up any peaks of other species, or the high dispersion of catalytic species placed on surface of the given support created microlitic or amorphous structure, which were unable to be detected by XRD spectrum.

The strong interaction between vanadium and tungsten species was further investigated via Raman spectra. The Raman spectra of dehydrated samples were collected from from 120 to 1100 $cm^{-1}$ (Fig.7). It revealed that the CC gave no distinct contribution to any Raman active bands, and therefore all the observed Raman peaks originated from supported coating layer. For sample V-W-Ti, four strong Raman peaks were observed at ca 150, 390, 508 and 627 $cm^{-1}$, which were associated with the

anatase phase[17,27] and brought into correspondence with sample $TiO_2$ (not given). These were exactly confirmed by XRD spectra. It was worth mentioning that strong Raman bands of anatase would impede the collection of the vibrational modes of surface vanadia species below 800 $cm^{-1}$.[18] As a result no Raman bands of vanadia species were observed except for the anatase over sample V-W-Ti.

By contrasting with sample V-W-Ti concerning the morphology of dispersed species, Sample V-W/Ti/CC undergone two main changes during a coating process. First, the most noticeable was an additional broad peak at the range of 870 to 1100 $cm^{-1}$ was observed, which was identified as vanadium and tungsten surface oxide species.[18] Secondly, the anatase Raman bands (observed at ca 150, 390, 508 $cm^{-1}$ respectively) were broader evidently than that of V-W-Ti, and the peaks blue shift (from 627 to 642 $cm^{-1}$) were observed.

Essentially, the coated catalyst with CC as support possessed of much higher surface metal atoms density for vanadium and tungten (~4.67 $V/nm^2$ and ~6.06 $W/nm^2$) than sample V-W-Ti (only 0.73$V/nm^2$ and 1.72$W/nm^2$). In general, the Raman peaks were affected by the loading amount of the active species, the more of it the more obvious of Raman peaks. In other words, the relative higher concentration of tungsta and vanadia than that of V-W-Ti made Raman give an information on tungsta and vanadia over sample V-W/Ti/CC. Additionally, the obvious enrichment of vanadium and tungsten in the coating layers resulted in anatase Raman bands broaden and blue shift, which meant as an arresting anatase crystal peak there had been depleting its grain seize.[19] We assumed that the pentavalent vanadium cation provided a smaller radius than tetravalent titania, which could be easily to make it motivate permeate and replace the tetravalent titanium cation over titania lattice, inducing titania lattice aberrance and crystal defect. Along with the increase of crystal defect the titania grains growth were restrained,[20,21] though it was not proved by any direct evidence. As previously reported,[8] one may decipher that the decrease of crystal grain size would induce its specific surface area increase.

Furthermore, the broad peak presented in the top right corner of the Fig5 depicted the information respecting the molecular structure of vanadia and tungsta in coatings. The overlapped peak was separated into three singlets, observed at ca 928, 984, 1012 $cm^{-1}$, respectively. A large literature suggested that below monolayer surface coverage (7~8$V/nm^2$) isolated monomeric, polymeric surface $VO_x$ species or support associated vibrations of the surface vanadia species were the dominant surface vanadia species.[18,22-24] And the morphostructure of the surface molecularly dispersed vanadia species were essentially independent of the oxide supports in their calcined, dehydrated state.[24] In our study, the peaks observed at ca 928 and 1012 $cm^{-1}$ were assigned to V–O–V stretching modes and V=O, respectively.[22-24] Burcham et al argued that two main Raman active bands at 1011~1040 and 840~940 $cm^{-1}$ were belonged to to a terminal V=O bond and polymerized V–O–V stretching modes of the surface molecularly dispersed vanadia species on dehydrated catalyst respectively.[24] Apparently, the observed band of 928 $cm^{-1}$ over the coated V-W/Ti/CC catalyst suggested the presence of polymeric surface vanadia species, and the proportion of polymerized surface vanadia species would be further investigated by UV-Vis DRS. By comparison with 840 $cm^{-1}$, the band of 928 $cm^{-1}$ indicated a prominent shifts upward, since the bridging V–O–V Raman band increases substantially with its coverage of surface vanadium atoms. Thus, we can surely argue that the surface $VO_x$ (vanadium atoms in the fully-oxidized) species were presented in isolated and polymeric state possessing one mono-oxo V=O terminal bond and three bridging V-O-M bands (M=V or support cation). Additionally, to the best of my knowledge, such species of vanadia were usually endowing with a higher performance in supported vanadia catalysts than the crystalline phases suppling fewer exposed active surface sites. The active band at ca 984 $cm^{-1}$ appeared in the dehydrated Raman spectra was perceived as octahedral coordination of tungsta species.[24] Yan et al argued that the typical octahedral structure of titania inducted surface tungsta species interacted with titania support to furnish a representative octahedral crystal lattice.[25]

In a word, the Raman spectra indicated that only surface vanadia and tungsta molecularly dispersed species were existed on this coated catalyst, and that greater sensitivity of Raman spectroscopy to the observation of crystalline vanadia and tungsta under a strong interference stemming from CC than did XRD

**Catalyst Redox Behavior Characterizations**

Table 2 Compositions of V-W/Ti/CC catalyst determined by XPS and XRF (at%).

| | O | Ti | W | V |
|---|---|---|---|---|
| XPS | 74.86 | 14.26 | 8.99 | 1.89 |
| XRF | 69.19 | 27.38 | 3.16 | 1.98 |

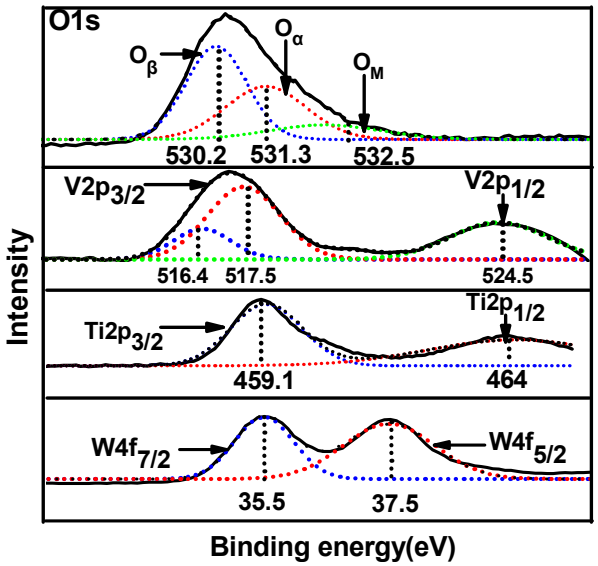


Fig. 6 XPS analysis of V 2p, Ti 2p, W 4f and O 1s over V-W/Ti/CC catalyst.

**XPS.** The composition of catalyst V-W-Ti/CC was investigated by XPS and XRF (Table 2). The values given by XPS represent surface atomic percentage measured in flaked solid, while XRF results indicate the bulk percentage measured in powder.

By comparison to the bulk concentrations obtained from XRF, surface tungsten atom percentage of the catalyst showed an upward trend from 3.16 at% to 8.99 at%, indicating an occurrence of surface tungsten enrichment. While a deeper

penetration of vanadia scattered around the bulk of the titania particles illustrated a homogeneous doping and distribution over the unit of $TiO_2/VO_x$-$WO_x/TiO_2$/CC analogous sandwich structure, which was concluded by the similar surface atom percentage with bulk of vanadia. According to the diffusion theory,[26] the diffusion distance of an extended source increases with the increase of its concentration. Sample V-W/Ti/CC possessed a atom percentage of 4.67 V/nm$^2$ and 6.06 W/nm$^2$, for sure, inner tungsta of the layer would be more easily enrich to surface. Additionally, the O/Ti+V+W atomic ratio calculated by XPS was 2.98, greater than 2.13 calculated by XRF, suggesting additional oxygen sources on the surface of catalyst were existed, since 2.98 represented a ratio that go far beyond the total stoichiometric proportion of vanadia, tungsta and titania.

Furthermore, the XPS of O 1s, V 2p, Ti 2p and W 4f spectra of V-W/Ti/CC samples were recorded and deconvoluted in Fig. 6. From Fig. 6, the O 1s spectra described a presence of three distinct O 1s peaks by searching for the optimum combination of Gaussian bands with the correlation coefficients ($R^2$) above 0.99 (Origin Pro, Version 8.5), indicating that there were three different oxygen sources on the surface. The sub-band at lower binding energy ca 530.2 eV originating from anatase titanium dioxide predominantly was attributed to the lattice oxygen denoted as $O_\beta$.[27-29] The one appearing at binding energy value ca 531.3 eV could be corresponded to the surface adsorbed oxygen denoted as $O_\alpha$,[29,31] such as $O_2^-$, $O^-$ belonging to defect-oxide.[29,30] The peak at high binding energy ca 532.5 eV was denoted as $O_M$ which was mainly for the contribution of O from the vanadium oxides and tungsten oxides. In general, the surface oxygen $O_\beta$ is more reactive in reactions due to its higher mobility than lattice oxygen $O_\beta$[31]. The experiment of temperature programmed desorption (TPD) observed a same desorption peak in any adsorption atmosphere, which presented something unlike the absorbed gas were existed inside sample V-W/Ti/CC. However, we were unable to detect the composition of desorption gas.

Deconvoluted V 2p photoelectron spectra showed a presence of three types of photoelectron peaks, V $2p_{3/2}$ B.E. of 517.5 eV and V $2p_{1/2}$ B.E. of 524.5 eV identified it as V(V), and V $2p_{3/2}$ B.E. of 516.4 eV identified it as V(IV). The results were agree well with the values reported in the literature.[32-34] The range of binding energy from 458 eV to 465 eV presented two well-defined peaks which ascribed Ti $2p_{3/2}$ (458.9 eV) and Ti $2p_{1/2}$ (464.8 eV) to characteristic Ti(IV).[32,33,35] The peaks of binding energies 35.5 eV and 37.5 eV were attributed to W $4f_{5/2}$ and W $4f_{7/2}$, respectively, which correspond well with characteristic of W(VI).[32,36] Neither titanium nor tungsten species exhibit any other valence states except their full oxide states after an elevated temperature calcination under the air condition, which indicated that the tungsta species were merely molecular dispersed instead of doping with titania lattice. However, the binding energy of V 2p and Ti 2p exerted a positive shift with respect to their pristine oxides, while the binding energy of W 4f shifted to low energy, according to the websits of XPSDATA and NIST. The fact that tungsta possessed a limited ability of capturing and transmitting electronic had been validated in great detail.[37-39] As a result, we assumed the tungsta species could attract the electron stemming from titania and vanadia, reducing the surrounding density of electron cloud of theirs', and promoted the electron transportation between vanadium species and titania, further facilitating vanadium species to generate a reduction state. Additionally, reduction profiles in the TPR measurements of the ternary catalysts V-W/Ti/CC were different from those expected by superimposing the profiles from the binary catalysts V/Ti/CC and W/Ti/CC, also indicating an interaction between vanadia and tungsta species.[40] (supporting information) Since if vanadia and tungsta species would exist independently on the titania surface, the reduction profile in the TPR measurements of the ternary catalysts would be expected to be a superimposition of the profiles of the corresponding binary systems.

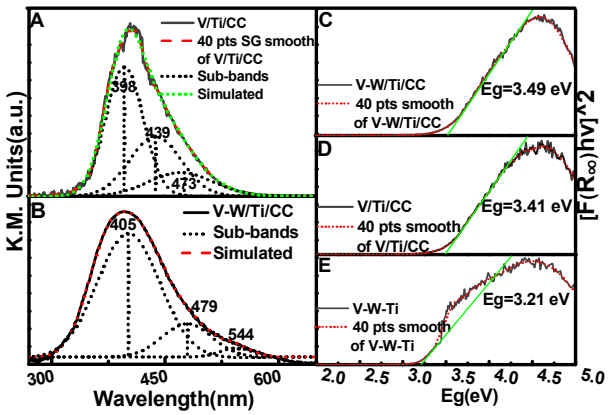


Fig. 7 Deconvoluted plots along with the Eg values of DRUV–Vis spectra.

**DRUV-vis.** The molecular structures of the supported vanadia phase on coating had been extensively characterized by XRD, XPS and Raman spectroscopic. While, DRUV-Vis spectroscopy is the most versatile spectroscopic technique in elucidating the structures and types of coated vanadia species by probing both ligand-to-metal ($O\rightarrow V^{5+}$) charge transfer (LMCT) transitions and the $V^{4+}$ spectra signal monitored with the d-d transition.[41-43] Although the directly chemical information are capable to be obtained by detecting the outer shell electrons. Nevertheless, we can still feel the least of perfection for DRUV-Vis, at least it is complex, and usually encompasses several broad and overlapping bands.[42]

In the present diagram, Fig 7A and Fig 7B were plotted by subtracting Ti/CC and W/Ti/CC bands from corresponding DRUV-Vis spectra aiming to distinguish and quantify the vanadium oxide as well as avoid spectral complications arising from something inessential. Under such circumstances, there was a asymmetric broad absorption for V-W/Ti/CC in the region of 300-600 nm (see Fig. 7B), of which four peaks corresponding to different types of vanadium species were observed. Particularly, the bands located at 405 and 479nm were assigned to $V^{5+}$ LCMT bands stemming from surface vanadia species both in monomeric and polymeric.[41-44] Additionally, the d-d transitions of $V^{4+}$ reduced vanadia cations for V-W/Ti/CC appeared as a weak and broad band at ca 544nm. Furthermore, for the purpose of clarifying the role of tungsta in the coated catalyst, we did a comparative trial using V/Ti/CC. Apparently, due to the deficiency of tungsten the band maximum of $V^{5+}$ LMCT peaks in V/Ti/CC exhibit a downshift in energy (see Fig 7A) accounting for the increasing extent of vanadia polymerization as a consequence of greater electron delocalization in polymerized structures.[42-44] In previously report, Bertinchamps et al argued that there was an accelerative role involving the supported tungsta in

strengthening the interaction between vanadia and titania, inhibiting vanadia polymerization, increasing the specific surface area, further to enhancing the performance of catalyst.[45] Accordingly, we hypothesis, the coated tungsta species owned a priority to occupy the adjacent octahedral titania vacant sites where an isolated vanadia species would interacted with their nearest isolated or polymeric vanadia species to generate polymeric vanadia species by bridging V-OV bonds. As a conclusion, the addition of coated tungsten oxides to the V/Ti/CC formulation squints towards promoting more isolated $VO_4$ units rather than polymeric $VO_3$ chains. It was also worth to noting that the peak at ~534 disappear indicating the coated tungsta facilitates to generate a vanadium species of reduction state confirmed by the result of XPS.

Here we further to quantified the rato of monomeric and polymeric surface vanadia species. According to the literature[46] that the absorption edge energy ($E_g$) could gave a deeper and more convenient elaborating of the electronic properties in solids sample than the UV-visible absorption spectra which could reflect the electronic structure of valence bands, but had difficulty in defining the position of these bands from the energy at maximum absorption since the the spectra of metal oxides possess broad nature of charge transfer features. In previous work, it had been proved that a linear function present between the $E_g$ and the number of bridging M-O-M bonds assumed in structures of the reference compound, which was independent of the local coordination except for the number of bridging M-O-M bonds, and that was analogous to the dehydrated surface $VO_4$ species existed in supported vanadia catalysts.[47,48] Tian et al[48] had developed a linear equation involving the Eg and the fraction of isolated surface vanadia structure, which was

$$E_g = 3.02 + 0.53\, X_m \quad \text{(eV)}$$

where $X_m$ refers to the fraction of monomer in sample, $E_g$ is determined by finding the x intercept of the straight line fitted through the low-energy using Tauc's law rise in the diagrams of $[F(R_\infty)\times h\nu]^2$ against hν, where $F(R_\infty)$ is the Kubelka–Munk function for powder samples extruded tabletting and hν is the energy of the incident photon.[41,44,46-48] The $E_g$ calculations given in Fig 7C, 7D and 7E were 3.49, 3.41 and 3.21, respectively. The fraction of polymeric surface vanadia in corresponding sample were 11.32%, 26.4% and 64.15%, respectively, which were well consistent with the qualitative analysis observed previously.

**Catalyst performance**

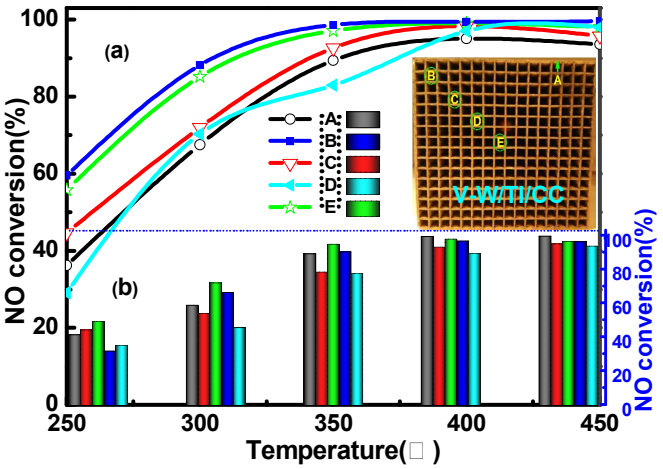


Fig. 8 NO conversion (a) and influence of $SO_2$ and $H_2O$ (b) in the $NH_3$-SCR reaction over different parts of V-W/Ti/CC catalyst. Conditions: (a) $[NH_3]=[NO]=500$ ppm, $[O_2]=2$ vol.%, $[SO_2]=1000$ ppm, $[H_2O]=10$ vol.%, $N_2$ balance and GHSV=6000 $h^{-1}$; (b) $[NH_3]=[NO]=500$ ppm, $[O_2]=2$ vol.%, $N_2$ balance and GHSV=6000 $h^{-1}$.

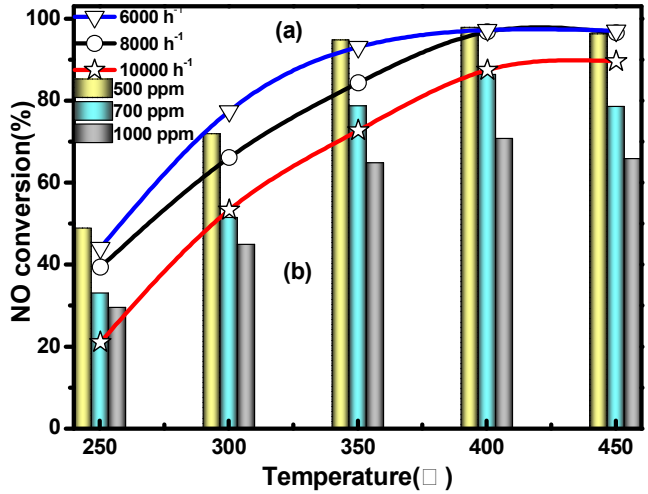


Fig. 9 Influence of space velocity (a) and concentration of NO (b) in the $NH_3$-SCR reaction over V-W/Ti/CC catalyst. Conditions: (a) $[NO]=[NH_3]=500$ ppm, $[O_2]=2$ vol.%, $N_2$ balance, (b) $[NH_3]=500$ ppm, $[O_2]=2$ vol.%, $N_2$ balance, GHSV=6000$h^{-1}$.

The serial catalysts sampled from different parts of V-W/Ti/CC were tested in the $NH_3$-SCR of NO as a function of NO conversion against temperature ranging from 250 to 450 ℃, and the results were shown in Fig 8(a). As was suggested from the graph, most of the catalysts exerted an excellent catalytic activity with a NO conversion exceeding 90% in the range of 350 ~ 450 ℃, even the catalyst sampled from the ektexine of honeycomb which was thicker than anywhere else exceeded 80%. For commercial V-W-Ti catalyst, the NO conversion ranged from 80% to 95% ( depends on the content of NO in inlet gas). Consequently, we thought the washcoat phase had formed a homogeneous distribution, ensuring the whole coated catalyst could be competent to the duty fulfilled by congeneric

well commercialized catalysts. Tolerant ability for $SO_2$ and steam poisoning were further tested and the result were showed in Fig 8(b). Obviously the NO conversion depicted a indifferent decrease contrasted with preceding performance, and surpasses 80% when temperature surpassed 350 □, revealing a strong resistance of water and $SO_2$ and potential value in industrial application. Furthermore, a relatively small amount of active washcoat phases for the V-W/Ti/CC meant a relatively finite catalytic capacity, which was suit for conditions with lower NO emissions, and resulting a faster response to changing conditions when NO concentration fluctuate from low to high with a corresponding increase in temperature. Necessarily, we investigated the changes of NO conversion over different NO concentration and space velocity. As we could see through Fig 9(a), the NO conversion decrease with increase of space velocity, especially leading to a sharp reducing in 10000 $h^{-1}$ of GHSV, which was unable to satisfy industrial demand. While the sample in 8000 $h^{-1}$ of space velocity achieved a desired anticipation with a NO conversion over 80% in the range of 350 ~ 450 □, though there was still a small flaw compared with sample in 6000 $h^{-1}$ of GHSV. Fig 9(b) showed that as the rising of temperature, the NO conversion indicated a decline from sharp to mild demarcated in the point of 350 □ when above 500 ppm NO concentration. Nevertheless, the NO conversion had already gone below 80% when temperature reach 450 □ over the samples in NO concentration of 700 ppm, even worse in higher NO concentration. In conclusion the coated catalysts presented a desired overall catalytic performance possessing NO elimination and excellent tolerance of $SO_2$ and steam in 8000 $h^{-1}$ of GHSV and 700 ppm NO concentration at most.

## Conclusions

In summary, we had dipped active materials onto cordierite to synthesis the monolithic V-W/Ti/CC catalyst which exhibited a desired catalytic performance together with a strong tolerance poisoning in sulfur and moisture. It was found that the washcoat obtained after the procedure of dip-coating, where structural collapse did not occurred instead preserving its previous porosity possessing mesopores and few new macropores in 3D network via a $N_2$ adsorption-desorption isotherms revealed a firm washcoat bonding reliability and a homogeneous distribution in the surface of cordierite. The catalyst components presented a state of fully-oxidized except for vanadia of which few tetravalent vanadium facilitated to be generated by the promotional effect of tungsten species on electron transportation between vanadium species and titanium support catalyst were consisted. The speciations of vanadia finely dispersed on support surfaces were mainly presented in isolated and polymeric state possessing one mono-oxo V=O terminal bond and three bridging V-O-M bands (M=V or support cation), and tungsta in octahedral coordination. A further investigation about the percent of polymeric vanadium oxide species indicated only minority vanadia species (ca 11.32w%) present a polymer.

## Acknowledgment

This work was supported by Wanshan hi-tech application engineering co, Ltd (no. 2013091620131216).

## Notes and references

*Chongqing Key Laboratory of Chemical Process for Clean Energy and Resource Utilization, College of Chemistry and Chemical Engineering (Chongqing), Chongqing University, Chongqing 400044, China. E-mail address: dujune@cqu.edu.cn. Phone: +86-13637765167. Fax, +86-23-65105106;

1. N. V. Economidis, D. A. Peria, P. G. Smirniotis, Appl. Catal., B, 1999, **23**, 123-134.
2. J. M. C. Buenoa, G. K. Bethkeb, M. C. Kungb and H. H. Kungb, Catal. Today, 1998, **43**, 101-110.
3. M. Kleemann, M. Elsener, M. Koebel and A. Wokaun, Appl. Catal., B, 2000, **27**, 231-242.
4. P.O. Thevenin, P.G. Menon, S.G. Järas, Cattech, 2003, **7**, 10-22.
5. O. Öhrman, J. Hedlund and J. Sterte, Appl. Catal., A,2004, **270**, 193.
6. H. Arai and M. Machida, Catal. Today, 1991, **10**, 81-94.
7. T. A. Nijhuis, A. E. W. Beers, T. Vergunst, I. Hoek, F. Kapteijn and J. A. Moulijn, Catal. Rev., 2001, **43**, 345-380.
8. J. F. Xu, G. X. Cheng and W. Yang, J. Phys., B, 1996, **29**, 6227-6232.
9. A. N. ShigaPov, G. W. Graham, R. W. Maeeabe and P. P. Michellene, Appl. Catal., A, 1999, **182**, 137-146.
10. Q. Liu, Z. Liu, Z. Huang and G. Xie, Catal. Today, 2004, **833**, 93-95.
10. E. G. Bordejé, L. Calvillo, M.J. Lázaro and R. Moliner, Appl. Catal., B, 2004, **50**, 235-242.
12. K. S. W. Sing, D. H. Everett, R. A. W. Haul, L. Moscou, R. A. Pierotti, J. Rouquerol, T. Siemieniewska, Pure & Appl. Chem., 1985, **57**, 603.
13. S. J. Gregg, K. S. W. Sing, Adsorption, Surface Area and Porosity; Academic: London, 997.
14. M. A. Kebede, M. E. Varner, N. K. Scharko, R. B. Gerber and J. D. Raff, J. Am. Chem. Soc., 2013, **135**, 8606-8615.
15. F. D. Liu and H. He, J. Phys. Chem,C, 2010, **114**, 16929-16936.
16. X. J. Yao, L Zhang, L. L. Li, L. C. Liu, Y. Cao, X. Dong, F. Gao, Y. Deng, C. J. Tang, Z. Chen, L. Dong and Y. Chen, Appl. Catal., B, 2014, 150, 315.
17. T. Ohsaka, F. Izumi and Y. Fujiki, J. Raman. Spectrosc., 1978, **7**, 321-324.
18. I. E. Wachs, Catal. Today, 1996, **27**, 437-455.
19. S. Kelly, F. H. Pollak and M. Tomkiewicz, J. Phys. Chem., B, 1997, **101**, 2730-2734.
20. T. J. Trentler, T. E. Denler and J. F.Bertone, J. Am. Chem. Soc., 1999, **121**, 1613-1614.
21. J. C. Parker and W. SiegelR, Appl. Phys. Lett., 1990, **57**, 943-945.
22. I. E. Wachs and B. M. Weckhuysen, Appl. Catal., A, 1997, **157**, 67.
23. G. Deo and I. E. Wachs, J. Catal., 1994, **146**, 323.
24. L. J. Burcham, G. Deo, X. T . Gao and I. E. Wachs, Top. Catal., 2000, **11/12**, 85-100.
25. Q. J. Yan and H. Y. Liu, J. Mol. Catal., 1988, **2**. 87.
26. J. Crank, The Mathematics of Diffusion, 2nd ed., Clarendon Press, Oxford, England, 1975, p. 15.
27. L. Q. Jing, X. J. Sun, W. M. Cai and X. Q. Li, Acta. Chim. Sci., 2003, **61**, 1241.
28. .M. Kumar, S. Badrinarayanan and M. Sastry, Thin Solid Films, 2000, **358**, 122.
29. M. Kang, E. D. Park, J. M. Kim and J. E. Yie, Appl. Catal., A, 2007, **327**, 261.

30. S. Azalim, R. Brahmi, M. Agunaou, A. Beaurain, J. M. Giraudon and J. F. Lamonier, Chem. Eng. J., 2013, **223**, 536-546.
31. H. Chen, A. Sayari, A. Adnot and F. Larachi, Appl. Catal., B, 2001, **32**, 195.
32. V. I. Bukhtiyarov, Catal. Today, 2000, **56**, 403-413.
33. S. Lars, T. Andersson, Catal, Lett., 1900, **7**, 351-358.
34. G. Hopfengärtnera, D. Borgmann, I. Rademacher, G. Wedler, E. Hums and G.W. Spitznagel, J. Electron. Spectrosc. Relat. Phenom., 1993, **63**, 91-116.
35. B. W. Callen, B. F. Lowenberg, S. Lugowski, R. N. S. Sodhi and J. E. Davies. J. Biomed. Mater. Res., 1995, **29**, 279-290.
36. G. E. McGuire, G. K. Schweitzer and T. A. Carlson, Inorg. Chem., 1973, **12**, 10.
37. D. N. Ke, H. J. Liu, T. Y. Peng, X. Liu and K. Dai, Mate. Lett., 2008, **62**, 447-450.
38. X. Z. Li, F. B. Li, C. L. Yang, and W. K. Ge, J. Photochem. Photobiol., A, 2001, **141**, 209-217.
39. S. L. Zhang and Q. Zhong. J. Mol. Catal., A, 2013, **373**, 108-113.
40. M. A. Reichea, T. Bürgi, A. Baiker, A. Scholz, B. Schnyder and A. Wokaun. Appl. Catal., A, 2000, 198, 155.
41. G. Catana, R. Ramachandra Rao, B. M. Weckhuysen, P. Van Der Voort, E. Vansant and R.A. Schoonheydt, J. Phys. Chem., B, 1998, **102**, 8005.
42. B. M. Weckhuysen and R. A. Schoonheydt, Catal. Today, 1999, **49**, 441-451.
43. A.B.P. Lever, Inorganic Electronic Spectroscopy (Elsevier, Amsterdam, 1968).
44. X. Gao, M. A. Banares and I. E.Wachs, J. Catal.,1999, **188**, 325.
45. F. Bertinchamps, C. Grégoire and E. M. Gaigneaux, Appl Catal., B, 2006, **66**, 10-22.
46. A. Khodakov, B. Olthof, A. T. Bell and E. Iglesia, J. Catal., 1999, **181**, 205-216.
47. X. Gao, and I. E.Wachs, J. Phys. Chem., B., 2000, **104**, 1261.
48. H. J. Tian, E. I. Ross, I. E. Wachs, J. Phys. Chem., B, 2006, **110**, 9593-9600.